ACS APPLIED MATERIALS & INTERFACES

Research Article

www.acsami.org

Drop Detachment and Motion on Fuel Cell Electrode Materials

Eric Gauthier, Thomas Hellstern, Ioannis G. Kevrekidis, and Jay Benziger*

Department of Chemical and Biological Engineering, Princeton University, Princeton, New Jersey 08544, United States

ABSTRACT: Liquid water is pushed through flow channels of fuel cells, where one surface is a porous carbon electrode made up of carbon fibers. Water drops grow on the fibrous carbon surface in the gas flow channel. The drops adhere to the superficial fiber surfaces but exhibit little penetration into the voids between the fibers. The fibrous surfaces are hydrophobic, but there is a substantial threshold force necessary to initiate water drop motion. Once the water drops begin to move, however, the adhesive force decreases and drops move with minimal friction, similar to motion on superhydrophobic materials. We report here studies of water wetting and water drop motion on typical porous carbon materials (carbon paper and carbon cloth) employed in fuel cells. The static coefficient of friction on these textured surfaces is comparable to that for smooth Teflon. But the dynamic coefficient of friction is several orders of magnitude smaller on the textured surfaces than on smooth Teflon. Carbon cloth displays a much smaller static contact angle hysteresis than carbon paper due to its two-scale roughness. The dynamic contact angle hysteresis for carbon paper is greatly reduced compared to the static contact angle hysteresis. Enhanced dynamic hydrophobicity is suggested to result from the extent to which a dynamic contact line can track topological heterogeneities of the liquid/solid interface.

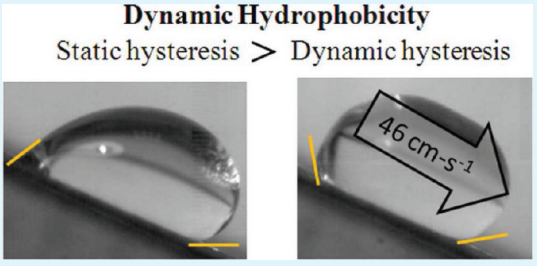

KEYWORDS: *contact angle, hydrophobic, carbon, wetting, carbon fibers, contact angle hysteresis, Teflon*

INTRODUCTION

Water transport is an essential element of polymer electrolyte membrane (PEM) fuel cell operation.[1−5] Liquid water that is formed at a catalyst/membrane interface is pushed through porous electrodes into gas flow channels. The water drops emerge from the largest pores in the electrode, and grow in the channel. Initially, the drops are held in place by adhesion to the water column in the electrode pore, but as the drops grow surface contact with the porous electrode and surface contact with the walls of the flow channel are the dominate adhesive forces. The drop must be detached and pushed through the gas flow channel in contact with the electrode surface to be removed from the fuel cell. Efficient fuel cell operation requires removal of liquid water drops from the fuel cell with minimal work. The surface properties of the porous electrode play a key role in the energy required to remove water drops from the gas flow channels of the fuel cell. We have been devising experiments to isolate the flow resistances for water transport through the porous electrode and gas flow channel.[6−8]

The porous electrode is required to carry the electron current from the electrocatalyst to the external circuit.[9] It must also permit transport of gas reactants and liquid product between the gas flow channels and the catalyst/PEM interface.[4,10,11] The porous electrode, or gas diffusion layer (GDL), of the fuel cell is typically made from carbon fibers, either as a random sheet of fibers in the form of carbon paper or as a woven array of fiber bundles forming carbon cloth.[12,13] These sheets of carbon fibers may be treated with adsorbed polymer layers to improve their function in fuel cells.[14,15] A thin layer of Nafion may be applied to the GDL where it contacts the catalyst layer to increase the three phase interface.[15] Teflon may be adsorbed onto the carbon fibers throughout the GDL to increase hydrophobicity and limit water accumulation within the porous carbon electrode. The structure and surface treatments of the carbon sheets affects the transport of water through the porous electrode, and has been the topic of many studies.[16−23] In addition, the structure and surface treatment of the GDL may affect the adhesion and motion of liquid water drops in the gas flow channel.

Figure 1 shows micrographs of typical carbon paper and carbon cloth used for fuel cell electrodes. The carbon fibers

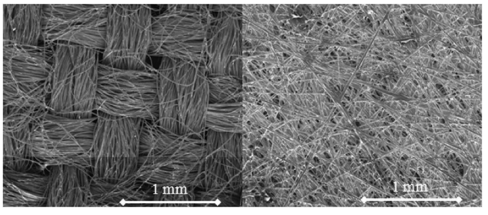

Figure 1. Scanning electron microscope images of carbon gas diffusion layer (GDL) materials. (a) Carbon cloth with 20% Teflon loading; (b) carbon paper with 20% Teflon loading.

making up these materials are ∼7−10 μm in diameter. They are randomly arranged in the carbon paper (Figure 1b). Porosimetry measurements show a typical pore diameter of 10−20 μm.[12,24] Carbon cloth has fiber bundles ∼400 μm in

Received: October 12, 2011
Accepted: December 27, 2011
Published: December 27, 2011

diameter. Porosimetry shows a bimodal pore size distribution with 10 μm pores between individual fibers and 100 μm pores at the intersection of fiber bundles.[12] Both carbon paper and carbon cloth are made hydrophobic with Teflon treatments. The carbon fiber sheets are impregnated with emulsions of Teflon, evaporating solvent and then annealing. The Teflon appears as webbing between the carbon fibers.

Theodorakakos et al. examined drop movement in fuel cell flow channels combined with contact angle hysteresis measurements.[25] Using the sessile drop method for contact angle determination they noticed a much larger contact angle hysteresis for carbon paper than carbon cloth and identified this as one of the key parameters limiting drop movement. (Static) contact angle hysteresis defines the degree to which a droplet must deform prior to movement; larger contact angle hysteresis suggests that greater force is required to initiate drop motion on carbon paper than carbon cloth. Both Chen et al.[26] and Kumbur et al.[27] examined the onset of drop motion from gas flow past the drop. They also related the onset of motion to the difference in advancing and receding contact angles.

The hysteresis between the advancing and receding contact angle of a material are determined by both the chemical properties of the material and the geometry of the rough surface.[28−31] Depending on the geometry, the hydrophobicity of a surface may be accentuated leading to superhydrophobicity.[32−36] Superhydrophobic surfaces display two qualities: 1) large contact angles with water, typically >150°; and 2) low contact angle hysteresis between the advancing and receding contact angles.[33] These qualities are indicative of low solid−liquid contact area compared to the drop area. Micron scale roughness of hydrophobic electrode materials can increase the contact angle with water, thus facilitating water removal from fuel cells.

In this paper, we report measurements of the static and dynamic interaction of water drops with Teflon, Nafion, graphite, and porous carbon sheets with different Teflon treatments. Advancing and receding contact angles were measured by a Wilhelmy plate method. Drop detachment due to gravity was measured as a function of drop size for the different surfaces employing a tilted plate. Lastly, drop motion on a tilted plate was measured as a function of tilt angle and drop size for water on the different surfaces. We show that the dynamic friction of water drops on the textured GDL surfaces is 2 orders of magnitude less than the static friction. We introduce the concept of dynamic hydrophobicity, arising when the moving contact line cannot respond fast enough to track changes in surface morphology; we will show that this reduces the dynamic contact angle hysteresis.

EXPERIMENTAL SECTION

Materials. The gas diffusion materials tested were purchased from Fuel Cell Earth LLC. Toray carbon paper materials (TGP-H-120) were obtained with treatments of 5, 20, and 40 wt % Teflon and a thickness of 370 μm. Woven carbon cloth was supplied by Fuel Cell Earth with 0, 20, and 40 wt % Teflon and a thickness of 380 μm. Teflon sheets (PTFE) and graphite composite were obtained from McMaster-Carr Supply. The PTFE sheets and graphite plates are the typical materials employed in machining bipolar plates and flow channels for fuel cells. Nafion 1110 membrane was obtained from Ion Power (New Castle DE).

Wilhelmy Plate Test. The advancing and receding contact angles were determined by the Wilhelmy Plate method with the samples of Teflon, graphite, Nafion or GDL initially suspended over deionized water from a bottom hanging analytical balance (Ohaus Model AR0640). The GDL was lowered into the water in increments of 127 μm every 10 s; this was sufficiently slow that the data represent static advancing and receding contact angles. The weight was recorded just prior to the moving the sample to the next position so that any dynamics of movement were eliminated. The sample was submerged to a depth of 7.5 mm and then the sample was raised at the same rate.

Drop Detachment. Drop detachment measurements were performed by depositing 20−80 μL drops on horizontal sheets 1 cm wide and 10 cm long. The sheets were supported on the plate attached to a rotary mount (Newport Corp.). The sample was tilted in increments of 1 degree and the minimum angle required for a droplet to begin moving and roll off the GDL was recorded. Photo images of the drop were obtained from the side and from the top. The aspect ratio of the drop width to length was measured immediately prior to detachment. The apparent contact angles were approximated for the sessile drops from the side images. The detachment angle measurement was repeated at least three times and averaged.

Drop Velocity. Drop velocity was determined by depositing a droplet on an inclined plane and video recording its movement using a Phantom-7 high speed camera over a distance of ~7 cm. The drop position was recorded as a function of time. Frame acquisition speed was adjusted according to the drop velocity. Frame rates of 30 frames per second were used for Teflon and graphite; drop motion on GDL materials was captured at 1000 frames per second. The apparent contact angles during drop movement were determined from the video images.

Drops were placed onto the inclined plane with a calibrated pipet. The drops were held in place by the pipet tip during deposition. Drop motion began when the pipet tip was removed from the drop.

RESULTS

Wilhelmy Plate Measurements. The contact angle is calculated via force balance in the Wilhelmy plate method,[31]

$$2\gamma_w L\cos\theta + (\text{buoyant force}) = \text{weight} \quad (1)$$

where γ_w is surface tension of water (72 mN m^{-1}) and L is the geometric length of the contact line ($L \approx 6.25$ cm, which is the perimeter of the sample). The buoyant force was determined from the linear region of the weight vs distance curve. The advancing and receding contact angles are shown in Figures 2 and 3.

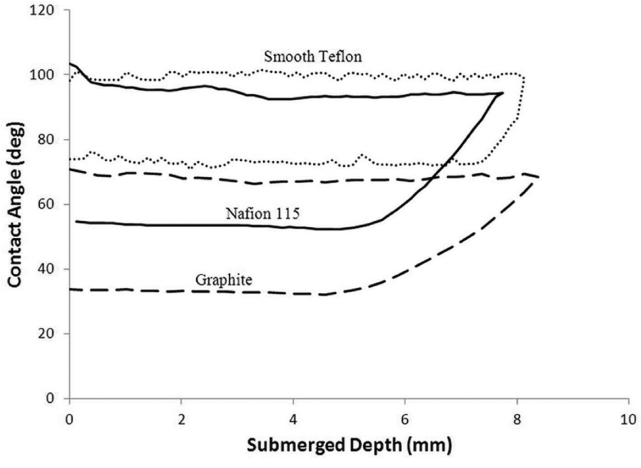

Figure 2. Advancing and receding contact angles measured by the Wilhelmy Plate method for Teflon, graphite composite, and Nafion.

Figure 4 shows a schematic of the sequence of the advancing and receding motion of the sample during the Wilhelmy plate measurement. Figure 2 shows results for Teflon, graphite and Nafion, while Figure 3 is for GDL materials. The advancing and receding contact angles are clearly depicted by the horizontal

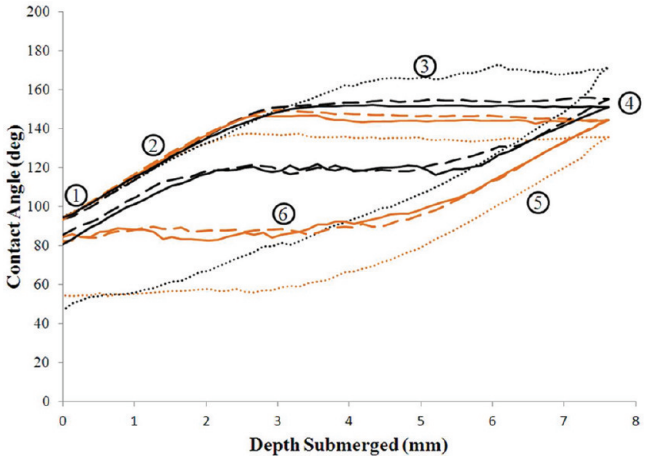

Figure 3. Advancing and receding contact angles measured by the Wilhelmy Plate method for carbon cloth with 0% (black dots), 20% (black dashes) and 40% (black solid line) Teflon loading, and carbon paper with 5% (orange dots), 20% (orange dashes) and 40% (orange solid line) Teflon loading. The points 1−6 correspond to the sequence shown in Figure 4.

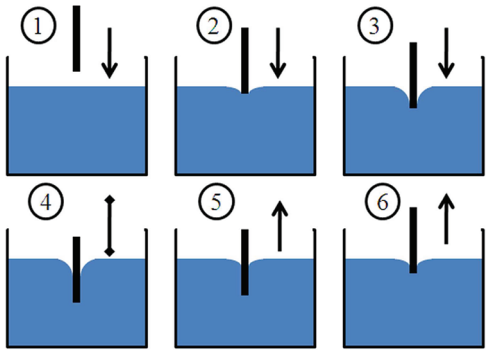

Figure 4. Wetting sequence for Wilhelmy Plate measurements with hydrophobic materials (contact angle >90°). The contact line gets pinned when the plate first enters the water, when it changes direction of motion and when it leaves the liquid.

regions (3 and 6 respectively in Figure 3). The regions when the contact angle is not constant occur when the sample is initially being submerged (region 2) and again when the sample is being withdrawn as the contact angle transitions from the advancing to receding angle as shown schematically as region 5 in Figure 4.

Teflon's advancing contact angle was ∼101° and receding contact angle was ∼73°. The advancing contact angles of Teflon in the literature range from 100 to 115°. The variations have been attributed to cleanliness and microscopic roughness. Graphite composite plates had an advancing contact angle of ∼68° and a receding contact angle of ∼35°. The contact angles for graphite are similar to those reported for individual carbon fibers.[37] Nafion is hydrophobic in the advancing direction with an advancing contact of angle of ∼95° and is noticeably hydrophilic in the receding direction with a contact angle of ∼50°. These values are similar to those previously reported by Goswami et al.[38]

The contact angles of water with GDL materials with and without Teflon treatments are significantly greater than those of Teflon and graphite. The larger contact angles for GDL materials are the result of only a fraction of the textured surfaces being wetted.[29,30,39−42] Carbon cloth has a larger advancing contact angle than carbon paper. The receding contact angle for carbon cloth is much greater than the receding contact angle for carbon paper. The contact angle hysteresis, which is the difference between the advancing and receding contact angles, is much larger for carbon paper than carbon cloth. The smaller contact angle hysteresis for carbon cloth we will attribute to the two-scale texture of the individual fibers and the fiber bundles, which will be discussed below.

The contact angle hystereses for 5% Teflon loaded carbon paper and 0% Teflon loaded carbon cloth are greater than those for 20% and 40% Teflon loaded carbon paper and carbon cloth respectively. The advancing contact angles of ∼140−160° are similar for all materials, but there are much larger differences between the receding contact angles. There is negligible structural difference between the carbon paper with different Teflon loading, suggesting that the difference is at the individual fiber contact angle level. On the individual fiber level, these materials are heterogeneous, consisting of Teflon regions and exposed carbon fiber. As the Teflon loading is increased from 5 to 20% the proportion of Teflon covering the surface increases. The composite contact angle will increase until the Teflon forms a homogeneous coating over the fiber. The data suggest that 20% and 40% Teflon loaded carbon paper had the carbon fibers fully covered with Teflon. At the 5% Teflon loading there were areas of the carbon surface that were not covered with Teflon and were less hydrophobic. This was even more evident in the receding contact angle for the 5% Teflon carbon paper which appeared to be hydrophilic.

Drop Detachment. The minimum tilt angle (α) is the smallest angle at which a drop will move spontaneously on a surface. By measuring the minimum tilt angle we can determine the force required to distort the drop shape and initiate movement. Figures 5−8 show the minimum tilt angles for drop

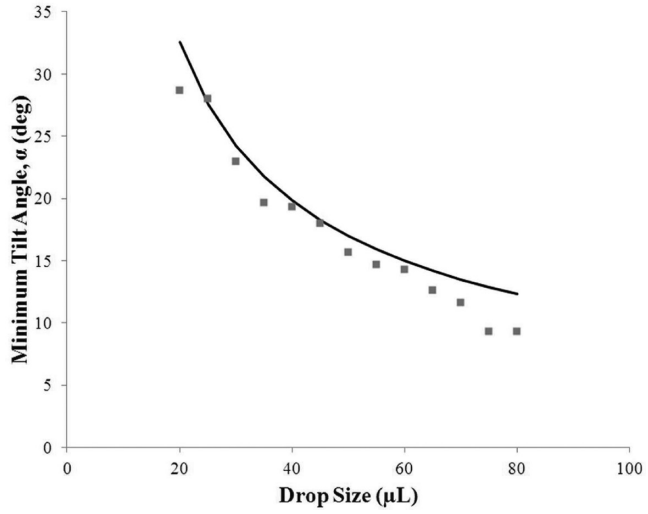

Figure 5. Minimum tilt angle for water drops to detach and move on PTFE surface (■). The line is the prediction of eqs 2 and 3, employing the advancing and receding contact angles determined from Wilhelmy plate measurements (θ_A = 101°, θ_R = 73°).

motion as a function of drop size on Teflon, Nafion and GDL surfaces. Drops smaller than a critical size will not detach from the surface.[33] (Even on a hydrophobic surface, the adhesive force for small drops is greater than gravity). As the surface is tilted the drop becomes elongated; this is seen in the top-view photos of drops presented in Figure 9. The photos of 70 μL

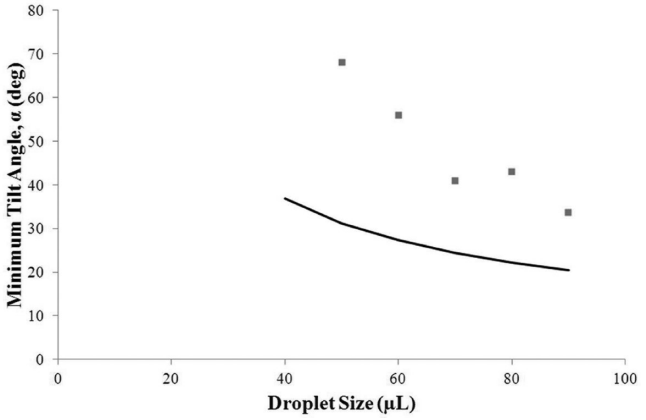

Figure 6. Minimum tilt angle for water drops to detach and move on Nafion surfaces (■). The Nafion 115 was a 127 μm thick Nafion membrane clamped to the tilted stage as both ends. The line is prediction based on eqs 2 and 3 employing the advancing and receding contact angles determined from Wilhelmy plate measurements (θ_A = 95°, θ_R = 50°).

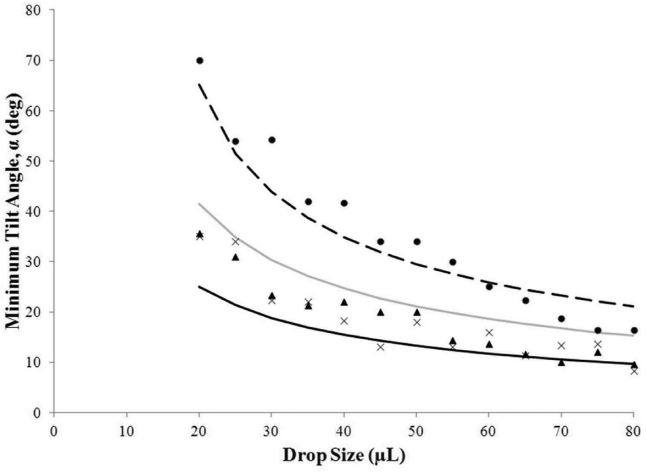

Figure 7. Minimum tilt angle for water drops to detach and move on carbon paper surfaces with 5% (●), 20% (▲) and 40% (×) Teflon loading. The lines are predictions based on eqs 2 and 3, employing the advancing and receding contact angles determined from Wilhelmy plate measurements (black dashed line: θ_A = 135°, θ_R = 56°) (gray solid line: θ_A = 143°, θ_R = 90°) (black solid line: θ_A = 143°, θ_R = 80°).

drops were used to estimate the drop ellipticity on Teflon, carbon paper, and carbon cloth surfaces.

The minimum tilt angles decreased with increasing drop volume as the gravitation force increased. The largest tilt angles were observed for the 5% Teflon-loaded carbon paper, which had the largest difference between the advancing and receding contact angles. Carbon paper with 20% and 40% Teflon loadings had the next largest tilt angles, slightly greater than the minimum tilt angle for Teflon. The 20% and 40% Teflon-loaded carbon cloth had the smallest minimum tilt angle, smaller than that for smooth Teflon.

The minimum tilt angle (α) for drop motion is where the force of gravity exceeds the differential force between the advancing and receding contact lines of the water drop with the solid surface, as given by eq 2, where ρ and V are the drop density and volume, w is the diameter of the drop where it contacts the horizontal surface, γ_w is surface tension of water,

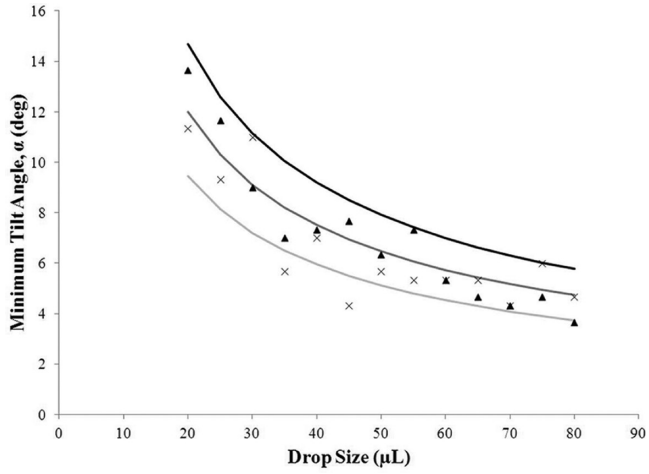

Figure 8. Minimum tilt angle for water drops to detach and move on carbon cloth surfaces with, 20% (▲) and 40% (×) Teflon loading. The lines are predictions of eqs 2 and 3, employing the advancing and receding contact angles determined from Wilhelmy plate measurements (light gray line: θ_A = 151°, θ_R = 128°) (black line: θ_A = 151°, θ_R = 122°) (light grey line: θ_A = 151°, θ_R = 117°).

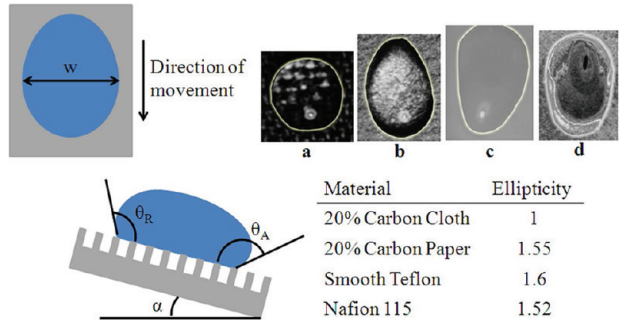

Material	Ellipticity
20% Carbon Cloth	1
20% Carbon Paper	1.55
Smooth Teflon	1.6
Nafion 115	1.52

Figure 9. Elongation of 70 μL drops on tilted surfaces just prior to detachment. (a) 20% Teflon loaded carbon cloth; (b) 20% Teflon loaded carbon paper; (c) PTFE surface, (d) Nafion surface.

and θ_A and θ_R are advancing and receding contact angles

$$\frac{\rho V g}{w}\sin(\alpha) = \gamma_w(\cos(\theta_R) - \cos(\theta_A)) \quad (2)$$

$$R = \left(\frac{3V}{\pi(1-\cos\theta_A)^2(2+\cos\theta_A)}\right)^{1/3}$$
$$w = 2R\sin\theta_A \quad (3)$$

The contact width of the drop in the direction of motion, w, is given by eq 3, where R is the radius of the spherical cap.

The critical detachment angle was estimated from eq 2 based on the advancing and receding contact angles determined from the Wilhelmy plate measurements. The contact width (w) for a spherical liquid cap contacting a solid surface with contact angle θ was evaluated using the approximation from Whyman, Bormashenko and Stein[43] given in eq 3. Extrand and Kumagai demonstrated that larger contact angle hysteresis was correlated with droplet ellipticity.[44] The effective contact width, w', in the direction of motion was also corrected for ellipticity, a_e=(drop length)/(drop width), assuming the same liquid−solid contact area as determined for the spherical cap, $w' = w/(a_e)^{1/2}$. Values for the ellipticity of drops on different surfaces are shown in Figure 9.

dx.doi.org/10.1021/am201408t | ACS Appl. Mater. Interfaces 2012, 4, 761−771

Equation 3 assumes that the drop grows on a horizontal surface in saturated vapor. As pointed out by Gao and McCarthy,[45] during evaporation or liquid withdrawal the drop radius (R) can be less than that predicted by eq 3; the lower limit for drop radius is defined by replacing θ_A with θ_R in eq 3.

The minimum tilt angles predicted from the force balances are plotted in Figures 5−8 along with the experimental measurements. There is good agreement between the experimental values and the predicted minimum tilt angles for all the materials except Nafion. Water drop adhesion to Nafion is much stronger than predicted from the contact angle hysteresis.

The critical angle for drop detachment is significantly greater for Teflon-treated carbon paper than the critical angles for smooth Teflon, suggesting that water drops adhere more strongly to Teflon- treated carbon paper GDL. But we observed that the drop velocity after detachment was orders of magnitude slower on smooth Teflon than on carbon paper. Furthermore, the drop velocities appeared to be similar on carbon paper and carbon cloth, even though they had much different detachment angles. This prompted a more detailed look at the drop motion after detachment.

Drop Motion on Inclined Surfaces. The distance drops travel as a function of time was determined for 30, 40, and 50 μL drops on smooth Teflon at tilt angles of 25−45° and on Teflon treated GDL materials at tilt angles of 20−30°. Drops were held in place by contact with the tip of the pipet used to deposit them. After the pipet tip was removed the drops began to move. The drop position as a function of time after removal of the pipet tip was determined from high speed video images. Typical data for Teflon, 40% Teflon treated carbon paper and 40% Teflon treated carbon cloth are shown in Figure 10.

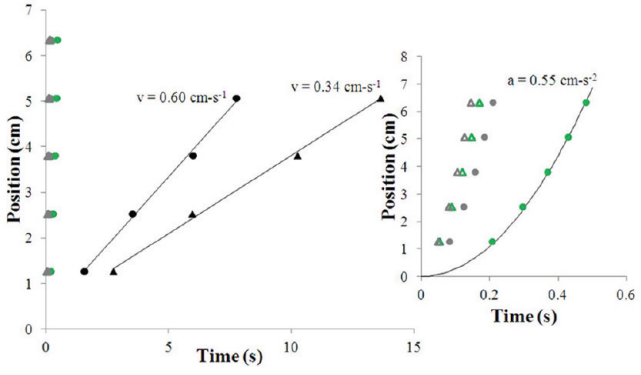

Figure 10. Displacement vs time for 50 μL drops moving down inclined planes of Teflon and GDL materials. Inset shows GDL data over shorter times. (Green circle: 20° tilt, 40% carbon paper; green triangle: 20° tilt, 40% carbon cloth; gray circle: 30° tilt, 40% carbon paper; grey triangle: 30° tilt, 40% carbon cloth; black circle: 45° tilt, smooth Teflon; black triangle: 40° tilt, smooth Teflon). The displacement vs time was fit to a constant velocity for drops on smooth Teflon and to a constant acceleration for the GDL materials.

Drops of this size kept accelerating on the GDL materials achieving velocities ~100 cm/s over 7 cm distance of travel. The acceleration was determined by fitting the displacement to $x = (1/2)at^2$. The accelerations as functions of drop size and tilt angle are summarized in Table 1.

In contrast to water drops moving on the textured GDL surfaces, water drops on smooth Teflon accelerate for a short period of time (<0.01 s) and then move at a constant velocity of 0.2−0.4 cm/s for tilt angles of 20−40°. Terminal velocities

Table 1. Acceleration of Water Drops on Gas Diffusion Materials

		acceleration (m s^{-2})				
drop size (μL)	tilt angle α (degrees)	no drag[a]	20% paper	40% paper	20% cloth	40% cloth
30	20	3.36	2.77	0.40	3.45	3.02
30	25	4.15	3.92	2.05	3.83	3.75
30	30	4.91	4.84	2.77	5.09	4.34
40	20	3.36	3.05	0.99	3.31	3.27
40	25	4.15	4.34	1.92	4.24	4.61
40	30	4.91	5.29	2.96	5.09	4.72
50	20	3.36	3.02	0.55	3.02	4.39
50	25	4.15	4.15	1.98	3.67	4.66
50	30	4.91	5.36	2.91	4.66	6.12

[a]Theoretical acceleration with no drag ($g\sin\alpha$).

were estimated from the displacement time data ($v_{drop} = \Delta x/\Delta t$). Thirty microliter water drops on carbon paper and carbon cloth also reached terminal velocities at 15° and 20° tilt angles. The data suggested that for larger tilt angles and larger drops the acceleration decreased as the drop velocity increased, but we were unable to track drop motion over a large enough distance to measure the terminal velocity. Table 2 summarizes

Table 2. Terminal velocities and Effective Drag Coefficient

material	drop size (μL)	tilt angle (degrees)	terminal velocity (cm s^{-1})	effective drag coefficient
20% carbon cloth	30	15	28	20
20% carbon paper	30	20	46	10
smooth Teflon	50	40	0.34	5×10^5
smooth Teflon	50	45	0.60	2×10^5

the terminal velocity data for smooth Teflon and the small drops at low tilt angles on carbon paper and carbon cloth. When drops achieve a terminal velocity, the force of gravity is balanced by the sum of the differential force of the advancing and receding contact lines, as given by eq 2, plus a drag force on the water drop by the surface on which it slides. An "effective" drag coefficient, η, was estimated from the terminal velocity and contact area of the drop with the surface as given by eq 4.

$$\begin{aligned} &(\text{drag force}) &&= (\text{gravity force}) \\ &&&\quad -(\text{moving contact line force}) \\ &\left(\tfrac{1}{2}\rho v_{drop}^2 \eta\left(Area\right)\right) &&\approx V_{drop}\rho g\sin\alpha \\ &&&\quad -w\gamma_w(\cos\theta_A - \cos\theta_R) \\ &\Rightarrow \eta \approx \frac{w^3\rho g\sin\ \alpha - w\gamma_w(\cos\theta_A - \cos\theta_R)}{\frac{1}{2}\rho v_{drop}^2 w^2} \end{aligned} \quad (4)$$

The effective drag coefficients were estimated based on the static contact angles determined from the Wilhelmy Plate measurements. The values calculated from eq 4 for water drops on smooth Teflon, and Teflon-coated carbon paper and carbon cloth are listed in Table 2. The effective drag coefficients predicted using static contact angles were 1×10^4 times larger

for smooth Teflon than those predicted for the Teflon-coated carbon fiber materials.

The displacement of the drop as a function of time was examined for several drops. After a water drop moved down a smooth Teflon surface a thin liquid film could be seen on left behind the trailing edge of the drop. Water drops on the GDL materials left no discernible liquid water on the surface after the drops moved past. There was no discernible difference in the drop motion between the first drop placed on the surfaces and a second or third drop placed on the surface. The drops on the fibrous GDL material surfaces showed no evidence of penetrating into the pores of the substrate and appeared to maintain constant volume with no loss of water as the drops moved.

Dynamic Contact Angles. Dynamic advancing and receding contact angles were estimated from the photos of the drops moving down the inclined plane. Shapes for static drops, just below the detachment tilt angle, and dynamic drops, just above the detachment tilt angle, are shown in Figure 11.

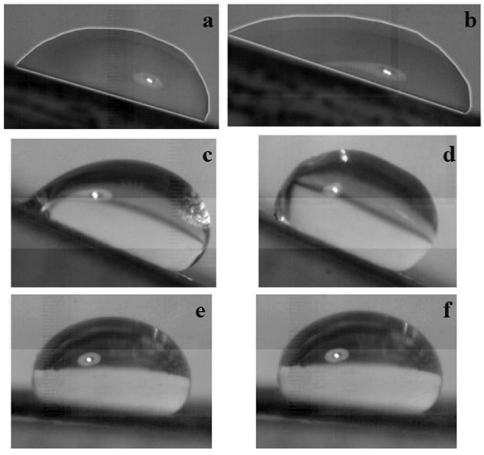

Figure 11. Static and dynamic water drops on inclined surfaces: (a) smooth Teflon, $\alpha = 18°$, $v = 0$ cm s^{-1}; (b) smooth Teflon, $\alpha = 18°$,$v <$ 1 cm s^{-1}; (c) 40% Teflon loaded carbon paper, $\alpha = 23°$, $v = 0$ cm s^{-1}; (d) 40% Teflon loaded carbon paper, $\alpha = 23°$, $v = 36$ cm s^{-1}; (e) 40% Teflon loaded carbon cloth, $\alpha = 7°$, $v = 0$ cm s^{-1}; (f) 40% Teflon loaded carbon cloth, $\alpha = 7°$, $v = 29$ cm s^{-1}; The photos were taken for 70 μL drops at tilt angles just below and just above the critical angle for drop detachment.

Table 3 compares static and dynamic contact angles for 70 μL drops on the different surfaces. The dynamic contact angles were averaged values, since the drop shapes fluctuated as the drops moved on the GDL surfaces. Figure 12 shows a photo sequence of a 70 μL drop moving on carbon paper at a 23° tilt

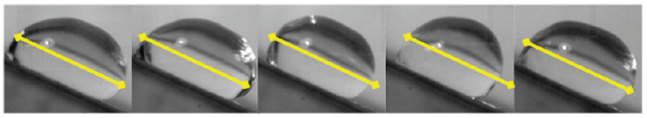

Figure 12. 70 μL water drop motion on 40% Teflon loaded carbon paper at at tilt angle of 23°, $v_{drop} \approx 36$ cm s^{-1}. The images are 0.01 s apart. The line across the waist of the drop is 6 mm.

angle; a 6 mm line drawn across the waist of the drop shows that the drop length fluctuated by 10−15%. We focus our attention on the contact angle hysteresis, defined as the difference between the advancing and receding contact angles. Results in Table 3 show that: (i) on smooth Teflon the dynamic contact angle hysteresis is larger than the static contact angle hysteresis $(\Delta\theta_{dynamic} > \Delta\theta_{static})_{Teflon}$; (ii) on carbon cloth the dynamic and static contact angle hystereses are about the same $(\Delta\theta_{dynamic} \approx \Delta\theta_{static})_{carbon\ cloth}$; and (iii) on carbon paper the dynamic contact angle hysteresis is reduced compared to the static contact angle hysteresis, $(\Delta\theta_{dynamic} < \Delta\theta_{static})_{carbon\ paper}$.

The observed drop accelerations were compared to those predicted from the force balance, given by eq 5 (which ignores drag on the drop). Force balances were compared both using the static contact angles (from Wilhelmy plate values) and the dynamic contact angles from the video images. Results are summarized in Table 4. Measured drop accelerations on carbon paper were much larger than those predicted by eq 5 based on the static contact angles; experimental drop accelerations were slightly less than the predicted values based on the dynamic contact angles. Drop accelerations on carbon cloth were slightly less than those predicted using either static or dynamic contact angles. Drop acceleration on smooth Teflon estimated from the static contact angles predicted drop velocities ~10 cm s^{-1}, more than an order of magnitude

Table 4. Comparison of Drop Acceleration

	acceleration (m-s^{-2})[a]			
	20% paper	40% paper	20% cloth	40% cloth
measured	2.0	0.45	1.5	2.2
force balance (dynamic contact angles)	2.3	1.0	2.6	2.7
force balance (static contact angles)	0.43	0.59	2.0	2.1

[a]Determined from video analysis of 50 μL drop and force balance accounting for dynamic and static contact angles of 50 μL drop (both methods are for 20° tilt angle).

Table 3. Static and Dynamic Contact Angles

		carbon cloth		carbon paper		
		20% Teflon	40% Teflon	20% Teflon	40% Teflon	smooth Teflon
static Wilhelmy plate	θ_A	153 ± 2	151 ± 3	147 ± 3	144 ± 3	99 ± 2
	θ_R	118 ± 3	118 ± 3	86 ± 3	87 ± 3	73 ± 3
static sessile drop[a]	θ_A	145 ± 5	148 ± 5	146 ± 5	149 ± 5	100 ± 5
	θ_R	116 ± 5	123 ± 5	57 ± 5	59 ± 5	64 ± 5
dynamic sessile drop[b]	θ_A	142 ± 5	141 ± 5	149 ± 8	130 ± 8	94 ± 5
	θ_R	107 ± 10	115 ± 10	114 ± 15	108 ± 15	33 ± 5

[a]Static contact angles from video images of 70 μL sessile drops at a tilt angle just prior to detachment. [b]Dynamic contact angles are for 50 μL drops moving on a surface at 20° tilt angle.

dx.doi.org/10.1021/am201408t | ACS Appl. Mater. Interfaces 2012, 4, 761−771

greater than those observed.

$$a = g\sin\alpha - \frac{\gamma w}{\rho V}(\cos\theta_R - \cos\theta_A) \quad (5)$$

The experimental drop accelerations on carbon paper and carbon cloth GDL surfaces with 20% Teflon loading were similar. Gravity quantitatively accounted for drop acceleration on the textured GDL surfaces; it appears that viscous drag of the moving drop is negligible. In contrast, water drop motion on smooth Teflon is much slower than that predicted by the force balance of gravity and surface tension, suggesting additional viscous drag is slowing down drop motion. This reinforces the results shown in Table 2 where the "effective" drag was 1×10^4 times greater for smooth Teflon than for carbon paper or carbon cloth.

The minimum tilt angle results suggest that water drops adhere more strongly to carbon paper GDL materials than to smooth Teflon. But the velocity at which the drops move after detachment suggests adhesion is somehow dramatically reduced for drops moving on the textured surfaces. This observation, coupled with the drop shapes from video images, indicated that the static and dynamic interfacial forces as represented by the contact angles are affected differently by surface topology.

The apparent dynamic contact angle hysteresis for carbon paper is significantly reduced compared to the static contact angle hysteresis, whereas the apparent dynamic contact angle hysteresis increased for smooth Teflon (refer to Table 3). Dynamic and static contact angle hysteresis was similar for woven carbon cloth with Teflon treatments. The textured carbon paper surfaces have a non-negligible static contact angle hysteresis that requires a substantial force to initiate motion, but once drops start to move the textured surfaces effectively act as thought they were very hydrophobic (almost superhydrophobic). We will refer to these Teflon-treated fibrous GDL materials as being dynamic-hydrophobic surfaces. (This is in contrast to "true" superhydrophobic surfaces that display near zero static as well as dynamic contact angle hysteresis.)

DISCUSSION

Water motion on the surfaces of fibrous carbon electrodes is critical to the operation of PEM fuel cells. It was intuitively obvious to chemists developing GDL materials that adding a thin layer of Teflon to the carbon fibers would make them more hydrophobic and facilitate the transport of water drops.[12,14,15,17,20,37,46,47] There are limits to the amount of Teflon that can be applied while maintaining good electrical conductivity of the material and allowing controlled permeability for gas and liquid water. It is rather amazing that the heuristic material design arrived at for GDL, which provided good lateral electronic conductivity while permitting transverse gas and liquid flows, also selected materials that permit drops to move on their surfaces with almost no resistance, i.e., the GDL materials display what we call dynamic-hydrophobicity. Dynamic-hydrophobicity combines chemical treatments and morphological structuring to control the strength and the extent of the liquid/solid interfacial contact for moving drops.

Over the past decade, preparation of superhydrophobic materials has garnered a great deal of attention. Water drops on such superhydrophobic surfaces require almost no force to initiate motion, and drops move with almost zero drag. These surfaces have contact angles of >150° and near zero static contact angle hysteresis. Specially structured surfaces with pillars of hydrophobic PDMS have been fabricated to have near zero static contact angle hysteresis.[32−35,48−56] Superhydrophobicity has been achieved by minimizing the contact points of the liquid drop with the solid surface, and ensuring that, at the points of contact, the surface is made hydrophobic ($\cos\theta \leq 0$).

Optimal micropatterned surfaces that are porous for transverse gas flow and continuous for lateral electronic conductivity would be complex to fabricate, which would make them expensive. But we can find structures in cheaper materials that mimic some of the characteristics of ideal superhydrophobic materials that can improve water transport on fuel cell electrodes. Specifically the forces required to both initiate and sustain drop motion should be minimized to reduce the parasitic power loss associated with water removal from PEM fuel cells.

Role of Surface Morphology on the Static Contact Angles. The contact angle measurements presented in Figures 2 and 3 show that: (1) Teflon is more hydrophobic than graphite; and (2) textured GDL surfaces are more hydrophobic than smooth Teflon surfaces. Teflon treated carbon paper and Teflon-treated carbon cloth both have advancing contact angles of ~150°. But the receding contact angle is much less for carbon cloth than carbon paper and the detachment angle is much greater for carbon paper than carbon cloth.

The effect of surface morphology on interfacial forces was first analyzed by Wenzel,[30] who attributed differences in adhesion to the effective liquid−solid contact area. This concept was refined by Cassie and Baxter;[29] many others have employed Cassie analysis to estimate the effective interfacial force between a liquid and a textured surface. Cassie and Baxter proposed that the contact angle for a textured surface (θ^*), given by eq 6, is the weighted average for liquid/solid interfacial energy (contact angle θ_{ls}) and the liquid/gas interfacial energy (contact angle 180°), where ϕ_s is the fraction of the solid surface contacting the liquid.

$$\gamma\cos\theta^* = \varphi_s\gamma\cos\theta_{ls} - (1 - \varphi_s)\gamma \quad (6)$$

Although the Cassie−Baxter approximation given by eq 6 has been extensively employed to model drops on textured surfaces it has also been extensively criticized; the criticism is that Cassie−Baxter uses area fractions for forces that exist along the perimeter of the contact line. This subtleties of this controversy is well treated by other authors.[45,57−59] We will employ the Cassie−Baxter approximation because of its simplicity and its intuitive approach to handle surface heterogeneities; but we must qualify our analysis because the limitations for applying the Cassie−Baxter approximation are not yet fully known.

The length scale of the texturing of GDL surfaces is critical to their hydrophobicity. To avoid water penetration into the space between the fibers of the GDL materials the distance between undulations in the surface (ζ) must be sufficiently small that water will only wet the outermost surfaces. Provided the contact angle is sufficient large water will not fill the voids between fibers, as shown in Figure 13. The depth d of the undulations must be greater than the liquid penetration depth resulting from the hydrostatic pressure head of the liquid drop pushing water into the void ($\Delta P_{drop} = \rho_w g R_{drop}$). The curvature of the water penetration into the undulation is given by the Young−Laplace equation. The critical radius of curvature, $R_{critical}$, at which the water will penetrate and touch the bottom

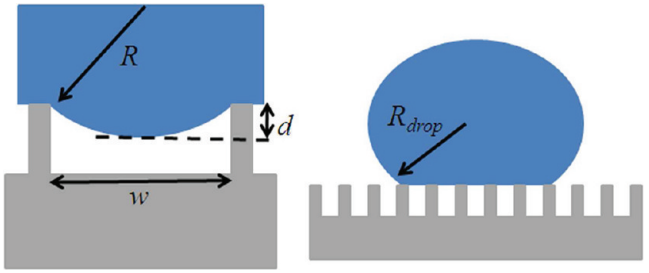

Figure 13. Schematic of water penetration into the undulations of a textured surface.

of the undulation, is given by eq 7.

$$R_{\text{critical}} = -\frac{2\gamma}{\Delta P} = -\frac{2\gamma_w \cos\theta}{\rho_w g R_{\text{drop}}} > \frac{(\zeta/2)^2 + d^2}{2d} = \frac{d}{2}(1 + (\beta/2)^2)$$

$$\beta = \zeta/d \tag{7}$$

The aspect ratio for surface texturing, β, which avoids liquid penetration, is given by eq 8.

$$\beta \geq 2\left[-\frac{4\gamma_w \cos\theta}{d\rho_w g R_{\text{drop}}} - 1\right]^{1/2} \tag{8}$$

The walls of the pores must be hydrophobic ($\cos\theta < 0$) for water drops to not penetrate into the GDL. The Teflon treatment makes the carbon fiber surfaces hydrophobic. The size of the drop also affects penetration. Larger drops result in larger hydrostatic pressures to force liquid into the pores. Assuming a contact angle of 101° for the Teflon coated fibers, water drops R_{drop} < 1 cm in diameter and the depth of the undulations equal to the fiber diameter (d = 10 μm) water will not penetrate undulations spaced less than 170 μm apart (ϕ_s > 0.08). For carbon paper water penetration should be negligible because the distance between carbon fibers must be much less than 100 μm in order to have reasonable electrical conductivity.

The typical flow channels in a fuel cell is 1 mm square, which limits the hydrostatic pressure to be even smaller than our conservative estimate given above. Once drops detach from the emergent pore in the GDL and begin to move it is expected there will be insignificant penetration of water drops or slugs into the pores of the GDL. A consequence of the absence of penetration of water into the pores is that the moving drops will maintain constant volume as they move along the surface of the GDL.

The 20 and 40% Teflon-loaded carbon paper surfaces may be modeled as solid surfaces of Teflon with air voids. The spacing between fibers is ~10–20 μm (see Figure 1), so there should be negligible water penetration into the voids. The contact angles with individual Teflon coated fibers should be equal to those for Teflon, θ_A = 101° and θ_R = 73°. The effective contact angles for the carbon paper are θ_A* = 144° and θ_R* = 87°. The area fraction of liquid/solid contact was estimated from the Cassie–Baxter equation for both advancing and receding contact angles. The solid fraction was calculated to be ϕ_s = 0.24 from the (macroscopic) advancing contact angle; this is in agreement with void fraction ($1 - \phi_s$)=0.75 of carbon paper previously measured by Benziger and co-workers.[6] The solid fraction was calculated to be ϕ_s = 0.81 from the (macroscopic) receding contact angle. The calculated liquid/solid contact area for the receding contact angles is larger than the liquid/solid contact area estimated from the advancing contact angles. We do not have a quantitative model to account for this difference; but Gao and McCarthy[45] pointed out that liquid detachment by disjoining at the receding contact line may not be well approximated by Cassie–Baxter analysis.

Carbon cloth has two-scale texturing. The individual fibers create a texture at the 10 μm scale. The fiber bundles create larger scale voids with a length scale of ~100 μm at the intersection of the fiber bundles, as seen Figure 1. A drop spanning the different scale texturing is schematically depicted in Figure 14. The distance of 100 μm is sufficiently small that

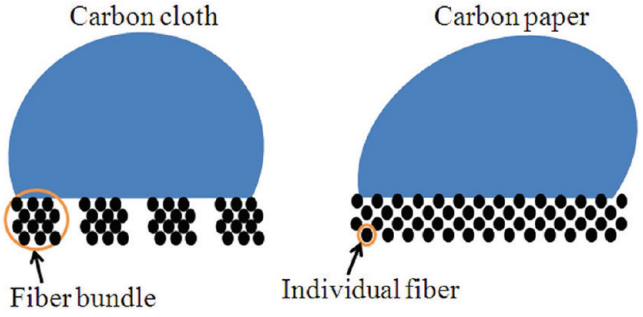

Figure 14. Schematic of the surface wetting of carbon paper and carbon cloth. The carbon paper shown to the right has uniform distribution of fibers with 10–20 μm undulations of the surface that are not wetted by water. Carbon cloth, shown at the left, has fiber bundles with 10 μm undulations and 100 μm void spaces at the intersections of the fiber bundles.

water should not significantly penetrate the voids. The solid fraction of the carbon cloth surface is similar to carbon paper. The effective liquid/solid contact was estimated to be 0.5 for both advancing and receding contact angles based on the Wilhelmy plate contact angles of θ_A** = 151 and θ_R** = 118° for carbon cloth and θ_A* = 144° and θ_R* = 87° for the carbon paper.

The static contact angle hysteresis (the difference between advancing and receding contact angles) is 33° for carbon cloth, which has two scale texture, and 57° for carbon paper, which has single scale texture. The advantage of the two-scale texturing over the single scale texturing is that it reduces the force required to detach water drops and cause them to move. The static adhesive forces of 50 μL drops on carbon paper and carbon cloth both with 20% Teflon loading are 24.9 and 9.7 mN, respectively. The 60% decrease in the force to detach the drops from carbon paper, compared to carbon cloth, will reduce the energy consumption associated with water removal from fuel cells.

Dynamic Contact Angles. Water drops on Teflon-treated carbon paper require more force to detach and move than water drops on smooth Teflon, yet after detachment, water drops move faster on carbon paper than on smooth Teflon. The difference in static adhesion between the two surfaces is consistent with the static contact angle hystereses measured by Wilhelmy plates. But the results in Table 2 show that the dynamic contact angle hysteresis is substantially reduced for the textured carbon paper surfaces relative to the static contact angle hysteresis. Why is there such a dramatic difference in the dynamic contact angle hysteresis for the textured surfaces?

We are not the first to report that textured or rough surfaces show dynamic hydrophobicity. A large number of papers have focused on superhydrophobic surfaces.[32−34,51−56,60,61] Those studies have employed microscale patterning with hydrophobic pillars and voids where liquid did not penetrate. They are different from what we report here. The superhydrophobic surfaces have vanishingly small static contact angle hysteresis and so they detach with almost no force. Sakai and co-workers have observed dynamic hydrophobicity for chemically patterned surfaces with hydrophobic patches.[62−65] They observed similar phenomena of a reduction of the adhesive forces for moving drops compared to static drops on chemically patterned surfaces. We have not seen reports in the literature of surfaces that display substantial barriers for initiating drop motion, but move almost frictionlessly after detachment.

We suggest that the transition from an adhesive static drop to a frictionless moving drop results from the inability of the moving liquid/solid contact line to track micrometer scale changes in surface morphology. The static drop achieves local shape equilibrium where the water/solid/vapor contact line can follow the microscale variations. But when the drop is moving, viscous forces and the liquid/vapor interfacial forces limit the ability of the contact line to follow morphological and compositional changes of the surface.

A simple model for a moving contact line can be developed by considering a surface with a patchwork pattern of different surface wetting properties, as illustrated in Figure 15. Provided

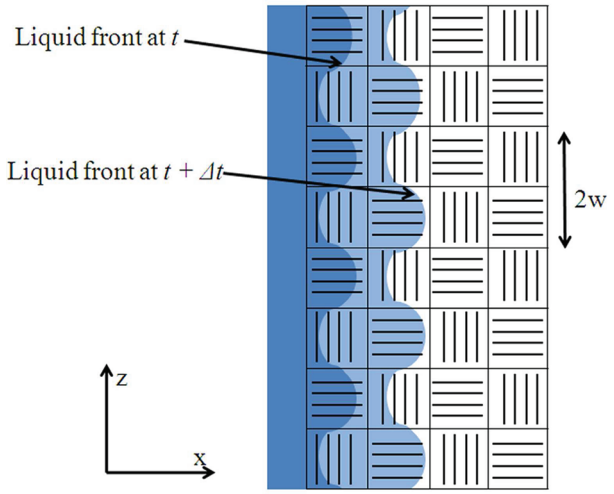

Figure 15. Schematic showing how the contact line oscillates as a drop moves over the patchwork surface of carbon cloth. The water drop is moving in the *x* direction.

the length scale of the patches is >1 μm, the liquid−solid−vapor contact can be treated macroscopically. Carbon cloth may be thought of as having patches ~400 μm square; each patch has the fibers oriented in a single direction with adjacent patches rotated by 90°. Carbon paper has a mesh of carbon fibers 10 μm across with 10 μm voids between the fibers. The local static contact angle of water with adjacent patches is different. At static conditions the local liquid−solid−vapor contact line will vary periodically in the *xz* direction (viewed from above) because of the locally periodically varying contact angle. The local liquid−solid surface contact line at constant z will also vary periodically in the *xy* direction (viewed from the side) because of the surface topology. Moving away from the solid−liquid−vapor contact line in the *y*-direction, the periodically varying curvature in the *z*-direction will eventually smooth out into the uniform drop shape with an apparent macroscopic contact angle θ^*. We will assume that the macroscopic apparent contact angle is a weighted average of the microscopic contact angles along the contact line. (This is the essence of the Cassie−Baxter equation).

When drops move in the *x*-direction, the solid−liquid−vapor contact line also advances. Advancing the drop by the characteristic length of surface undulations, ζ, shifts the phases of the contact line undulations by 180°. Drop motion on the textured surface will produce a periodic pressure fluctuation at the solid−liquid−vapor contact line that we expect to give rise to traveling capillary waves that move away from the contact line across the surface of the drop. If the frequency of the traveling waves is too large they will be attenuated, (i.e., surface tension and viscosity will act as a high frequency filter).

On the basis of dimensional analysis, the frequency of capillary waves should scale with liquid surface tension, liquid density and drop size as shown in eq 9.[50] Microliter water drops have a resonance frequency of ~40 Hz.

$$\nu_{\text{capillary}} \approx \left(\frac{\gamma_w}{\rho_w V_{\text{drop}}}\right)^{1/2} = 38\ \text{s}^{-1} \tag{9}$$

The driving frequency for the surface waves caused by drop motion is the drop velocity (v_{drop}) divided by the distance between undulations, *w*, as shown in eq 10. Drops moving at 10 cm-s^{-1} with distances between undulations of 400 μm (carbon cloth) or 10 μm (carbon paper) drive wave formation along the liquid/solid/vapor contact line at frequencies 5−200 times greater than the natural frequency for capillary waves to move across the drop surface. As the water drops slide down the inclined surface, the periodic variations along the contact line are damped out by water's surface tension. Because the advancing and receding contact line variations are damped, the contact angle hysteresis is also reduced.

$$\nu_{\text{driving}} = \frac{v_{\text{drop}}}{\zeta} = \begin{cases} 250\ \text{s}^{-1}(\text{carbon cloth}) \\ 8000\ \text{s}^{-1}(\text{carbon paper}) \end{cases} \tag{10}$$

The amplitude of the effective contact angle difference between the liquid−solid and liquid−void patches will be attenuated when the drop motion is driving wave formation at a frequency much greater than the natural frequency for capillary waves. The attenuation is expected to be greater for small separations between undulations. The carbon paper has smaller separation, resulting in higher frequency of wave propagation, which is attenuated more. Carbon paper shows a larger difference between static and dynamic contact angle hysteresis than carbon cloth, consistent with the difference in spacing between their respective undulations. Equation 9 suggests that the natural frequency for capillary waves decreases with drop volume. This is consistent with the experimental results for drop acceleration given in Table 1; smaller drops accelerate less because the capillary wave attenuation is reduced for smaller drops as evidenced by the observed dynamic contact angles. Smaller drops should also accelerate less because they have larger perimeter to volume ratios (refer to eq 5).

Nosonovsky has suggested that drops rolling down a rough surface may "bounce" giving rise to dynamic hydrophobicity.[66] Our data show accelerations very close to $g\sin\alpha$, which is

indicative of sliding. For drops to roll, there would have to be friction, and the drops' acceleration would be reduced.

Quéré and co-workers[33] reported that gravity scaling for drops on superhydrophobic surfaces is given by eq 11. They assumed, as have other investigators, that the dynamic contact angles are well-approximated by the static contact angles.

$$a \approx g\left(1 - \frac{\gamma}{\rho g}\frac{\pi\left(1 - \frac{\theta_A + \theta_R}{360^0}\right)}{w^2}(\cos\theta_A - \cos\theta_R)\right)\sin\alpha \quad (11)$$

Quéré's analysis indicated that on superhydrophobic surfaces drop acceleration increases with decreasing drop size (w), drop acceleration increases with contact angle ($(\theta_A + \theta_R)/2$) and drop acceleration increases with decreasing contact angle hysteresis ($\cos\theta_A - \cos\theta_R$). Dynamic-hydrophobicity, reported here, follows trends opposite those for superhydrophobicity. When we compared 20% Teflon loaded carbon paper and carbon cloth, every one of those predictions based on static contact angles is violated; smaller drops accelerated more slowly, drops accelerated faster on carbon paper which had a smaller average contact angle and drops accelerated faster on carbon paper which showed a larger static contact angle hysteresis.

Results summarized in Table 3 indicate that the dynamic advancing and receding contact angles are not equally affected by drop motion. The difference between advancing and receding contact angles is also evident in the images for static and moving drops on carbon paper shown in Figure 10. The advancing contact angles are affected less by drop motion than the receding contact angles. The dynamic advancing contact angle on smooth Teflon was only 5° less than the static contact angle, yet the receding contact angle was reduced by 31°. The advancing contact angle decreased 10−20° on carbon paper, but the receding contact angle increased by 40−50°. Gao and McCarthy[45] pointed out that physical forces in the advancing and receding directions are not symmetrical, which appears to also be the case for the changes induced by drop motion.

Anomalous Case of Drop Detachment from Nafion. Nafion is sometimes added with Teflon to coat the carbon fibers and provide for proton transport to and from the fiber surface. We included surface wetting of Nafion by water in this study for completeness. The results for drop detachment on Nafion were surprising. The critical tilt angle for drop detachment could be accurately predicted for Teflon, carbon paper, and carbon cloth surfaces based on the Wilhelmy plate measurements of the static advancing and receding contact angles. However, the water drops adhered to Nafion with much greater force than suggested by the static advancing and receding contact angles. Previous work by Goswami et al. suggested that the surface composition of Nafion is altered by the presence of liquid water.[38] Nafion is a microphase separated copolymer of hydrophilic and hydrophobic domains. Goswami et al. suggested that when the Nafion surface is exposed to a dilute gas phase (with or without water vapor) the surface is enriched in the lower energy hydrophobic components. Nafion surfaces exposed to liquid water have hydrophilic domains drawn to the surface to which water strongly adheres. The area under the drop is hydrophilic resulting in a greater adhesive force than if the surface was exposed to a vapor. The receding contact line is exposed to a hydrophilic surface (over which the drop just moved), so that the static contact angle hysteresis is greater than predicted from a uniform Nafion surface composition.

CONCLUSIONS

The major result from this study is that fibrous carbon electrodes coated with Teflon display dynamic-hydrophobicity; water drops adhere strongly to carbon cloth and carbon paper at static equilibrium, but move almost frictionlessly once they start to move.

This study presented detailed measurements of advancing and receding contact angles, water drop detachment and water drop motion on Teflon, graphite, Nafion, and Teflon-modified carbon paper and carbon cloth. Key results are:

(1) The static advancing and receding contact angles for Teflon-treated carbon cloth and carbon paper are greater than the contact angles of smooth graphite and smooth Teflon.

(2) The detachment of water drops from Teflon, carbon paper, and carbon cloth surfaces is accurately predicted from the static contact angle hysteresis of water on those surfaces. The detachment of water drops from Nafion is not accurately predicted. The failure to predict water detachment from Nafion is suggested to result from different chemical surface compositions under the water drop and outside the drop perimeter.

(3) After detachment, water drops move slowly down smooth Teflon surfaces achieving terminal velocities of ~0.1−1 cm s^{-1}.

(4) After detachment water drops accelerate with little friction on carbon paper and carbon cloth surfaces. Drops accelerate to velocities approaching 100 cm s^{-1}.

(5) (a) The dynamic contact angle hysteresis is greater than the static contact angle hysteresis for water drops on smooth Teflon; (b) the dynamic and static contact angle hystereses are similar for Teflon-treated carbon cloth; (c) the dynamic contact angle hysteresis is less than the static contact angle for Teflon-treated carbon paper.

(6) Dynamic hydrophobicity, where dynamic friction is significantly reduced compared to static friction on textured surfaces, has been proposed to result from attenuation of capillary waves created as drops move across a solid surface with local heterogeneities.

Initiating drop movement in fuel cell flow channels contributes to parasitic losses and reduced system power density. Surface texturing is shown to be beneficial to the speed of drop movement and the force necessary to initiate drop motion. The dynamic-hydrophobic effect reported here could assist in designing rough surfaces for the flow channel walls in PEM fuel cells. Sizing of the texturing features is critical. Two-scale texturing can reduce both the work to detach drops and the work to push drops along a surface.

AUTHOR INFORMATION

Corresponding Author

*Phone: 609-258-5416. Fax: 609-258-0211. E-mail: benziger@princeton.edu.

ACKNOWLEDGMENTS

The authors thank funding by NSF (CBET-0754715), the Princeton Center for Complex Materials NSF DMR-0819860 and the Department of Energy (DE-SC-0002097). We also thank Qiongjuan Duan and Theodore Charles for experimental assistance.

REFERENCES

(1) Mench, M. *Fuel Cell Engines*; Wiley: Hoboken, NJ, 2008.
(2) Barbir, F. *PEM Fuel Cells: Theory and Practice*; Elsevier Academic Press: Burlington, MA, 2005.
(3) Konrad, G.; Sommer, M.; Loschko, B.; Schell, A.; Docter, A. *A Handbook of Fuel Cells*; Wiley: Indianapolis, 2003; Vol. *4*.
(4) Pasaogullari, U.; Wang, C. Y. *J. Electrochem. Soc.* **2004**, *151*, A399−A406.
(5) Kordesch, K. K.; Oliveira, J. C. T. In *Ullman's Encyclopedia of Industrial Chemistry*; Elvers, B., Hawkins, S., Schulz, G., Ravenscroft, M., Rounsaville, J. F., Eds.; VCH: New York, 1985; Vol. *A12*, p 55−83.
(6) Benziger, J.; Nehlsen, J.; Blackwell, D.; Brennan, T.; Itescu, J. *J. Membr. Sci.* **2005**, *261*, 98−106.
(7) Gauthier, E.; Hellstern, T.; Benziger, J. *Fuel Cells* **2012**, submitted.
(8) Colosqui, C. E.; Cheah, M. J.; Kevrekidis, I. G.; Benziger, J. B. *J. Power Sources* **2011**, *196*, 10057−10068.
(9) Meng, H.; Wang, C. Y. *J. Electrochem. Soc.* **2004**, *151*, A358−A367.
(10) Weber, A. Z.; Newman, J. *Chem. Rev.* **2004**, *104*, 4679−4726.
(11) Wang, C.-Y. *Chem. Rev.* **2004**, *104*, 4727−4766.
(12) Mathias, M.; Roth, J.; Fleming, J.; Lehnert, W. In *Handbook of Fuel Cells−Fundamentals, Technology and Applications*; Vielstich, W., Gasteiger, H., Lamm, A., Eds.; John Wiley & Sons: Chichester, 2003; Vol. 3: Fuel Cell Technology and Applications, p 517−537.
(13) Wang, C. Y. In *Handbook or Fuel Cells*; Vielstich, W., Gasteiger, H., Lamm, A., Eds.; Wiley & Sons Ltd.: Chichester, 2003; Vol. *3*, p 337−348.
(14) Park, G. G.; Sohn, Y. J.; Yang, T. H.; Yoon, Y. G.; Lee, W. Y.; Kim, C. S. *J. Power Sources* **2004**, *131*, 182−187.
(15) Ma, J. X.; Yi, B. L.; Yu, H. M.; Hou, Z. J.; Zhang, H. M. *Prog. Chem.* **2004**, *16*, 804−812.
(16) Song, J. M.; Cha, S. Y.; Lee, W. M. *J. Power Sources* **2001**, *94*, 78−84.
(17) Lobato, J.; Canizares, P.; Rodrigo, M. A.; Ruiz-Lopez, C.; Linares, J. J. *J. Appl. Electrochem.* **2008**, *38*, 793−802.
(18) Kannan, A. M.; Cindrella, L.; Munukutla, L. *Electrochim. Acta* **2008**, *53*, 2416−2422.
(19) Friedmann, R.; Van Nguyen, T. *J. Electrochem. Soc.* **2010**, *157*, B260−B265.
(20) Fairweather, J. D.; Cheung, P.; Schwartz, D. T. *J. Power Sources* **2010**, *195*, 787−793.
(21) Xie, J.; Garzon, F.; Zawodzinski, T.; Smith, W. *J. Electrochem. Soc.* **2004**, *151*, A1084−A1093.
(22) Zamel, N.; Li, X. G.; Becker, J.; Wiegmann, A. *Int. J. Hydrogen Energy* **2011**, *36*, 5466−5478.
(23) Abaoud, H. A.; Ghouse, M.; Lovell, K. V.; Al-Motairy, G. N. *J. New Mater. Electrochem. Syst.* **2003**, *6*, 149−155.
(24) Kumbur, E. C.; Sharp, K. V.; Mench, M. M. *J. Electrochem. Soc.* **2007**, *154*, B1295−B1304.
(25) Theodorakakos, A.; Ous, T.; Gavaises, A.; Nouri, J. M.; Nikolopoulos, N.; Yanagihara, H. *J. Colloid Interface Sci.* **2006**, *300*, 673−687.
(26) Chen, K. S.; Hickner, M. A.; Noble, D. R. *Int. J. Energy Res.* **2005**, *29*, 1113−1132.
(27) Kumbur, E. C.; Sharp, K. V.; Mench, M. M. *J. Power Sources* **2006**, *161*, 333−345.
(28) Cassie, A. B. D. *Trans. Faraday Soc.* **1948**, *44*, 11−16.
(29) Cassie, A. B. D.; Baxter, S. *Trans. Faraday Soc.* **1944**, *40*, 0546−0550.
(30) Wenzel, R. N. *Ind. Eng. Chem.* **1936**, *28*, 988−994.
(31) Adamson, A.; Gast, A. *Physical Chemistry of Surfaces*, 6th ed.; Wiley: New York, 1997.
(32) Reyssat, M.; Quere, D. *J. Phys. Chem. B* **2009**, *113*, 3906−3909.
(33) Reyssat, M.; Richard, D.; Clanet, C.; Quere, D. *Faraday Discuss.* **2010**, *146*, 19−33.
(34) Gao, L.; McCarthy, T. J.; Zhang, X. *Langmuir* **2009**, *25*, 14100−14104.
(35) Gao, L. C.; Fadeev, A. Y.; McCarthy, T. J. *MRS Bull.* **2008**, *33*, 747−751.
(36) Leidenfr.Jg *Int. J. Heat Mass Transfer* **1966**, *9*, 1153-&.
(37) Wood, D. L.; Rulison, C.; Borup, R. L. *J. Electrochem. Soc.* **2010**, *157*, B195−B206.
(38) Goswami, S.; Klaus, S.; Benziger, J. *Langmuir* **2008**, *24*, 8627−8633.
(39) Johnson, R. E.; Dettre, R. H. *J. Phys. Chem.* **1964**, *68*, 1744-&.
(40) Johnson, R. E.; Dettre, R. H. In *Contact Angle, Wettability, and Adhesion*; Fowkes, F., Ed.; American Chemical Society: Washington, D.C., 1964; p 112−135.
(41) Johnson, R. E.; Dettre, R. H. In *Contact Angle, Wettability,and Adhesion*; Fowkes, F., Ed.; American Chemical Society: Washington, D.C., 1964; p 136−144.
(42) Johnson, R. E.; Dettre, R. H. *J. Colloid Sci.* **1965**, *20*, 173-&.
(43) Whyman, G.; Bormashenko, E.; Stein, T. *Chem. Phys. Lett.* **2008**, *450*, 355−359.
(44) Extrand, C. W.; Kumagai, Y. *J. Colloid Interface Sci.* **1995**, *170*, 515−521.
(45) Gao, L. C.; McCarthy, T. J. *Langmuir* **2006**, *22*, 6234−6237.
(46) Thoben, B.; Siebke, A. *J. New Mater. Electrochem. Syst.* **2004**, *7*, 13−20.
(47) Lim, C.; Wang, C. Y. *Electrochim. Acta* **2004**, *49*, 4149−4156.
(48) Gao, L.; Fadeev, A. Y.; McCarthy, T. J. *MRS Bull.* **2008**, *33*, 747−751.
(49) Gao, L.; McCarthy, T. J. *J. Am. Chem. Soc.* **2006**, *128*, 9052−9053.
(50) Gao, L.; McCarthy, T. J. *Langmuir* **2009**, *25*, 14105−14115.
(51) Krumpfer, J. W.; Bian, P.; Zheng, P. W.; Gao, L. C.; McCarthy, T. J. *Langmuir* **2011**, *27*, 2166−2169.
(52) Krumpfer, J. W.; McCarthy, T. J. *Faraday Discuss.* **2010**, *146*, 103−111.
(53) Lin, Y.; Ehlert, G. J.; Bukowsky, C.; Sodano, H. A. *ACS Appl. Mater. Interfaces* **2011**, *3*, 2200−2203.
(54) Miwa, M.; Nakajima, A.; Fujishima, A.; Hashimoto, K.; Watanabe, T. *Langmuir* **2000**, *16*, 5754−5760.
(55) Sheng, X.; Zhang, J. *Appl. Surf. Sci.* **2011**, *257*, 6811−6816.
(56) Wang, J.; Liu, F.; Chen, H.; Chen, D. *Appl. Phys. Lett.* **2009**, 95.
(57) Oner, D.; McCarthy, T. J. *Langmuir* **2000**, *16*, 7777−7782.
(58) Gao, L. C.; McCarthy, T. J. *Langmuir* **2007**, *23*, 3762−3765.
(59) Nosonovsky, M. *Langmuir* **2007**, *23*, 9919−9920.
(60) Bhushan, B.; Jung, Y. C.; Koch, K. *Philos. Trans. R. Soc. London, Ser. A* **2009**, *367*, 1631−1672.
(61) Hsieh, C.-T.; Chen, W.-Y. *Surf. Coat. Technol.* **2011**, *205*, 4554−4561.
(62) Furuta, T.; Sakai, M.; Isobe, T.; Matsushita, S.; Nakajima, A. *Langmuir* **2011**, *27*, 7307−7313.
(63) Sakai, M.; Song, J. H.; Yoshida, N.; Suzuki, S.; Kameshima, Y.; Nakajima, A. *Surf. Sci.* **2006**, *600*, L204−L208.
(64) Song, J. H.; Sakai, M.; Yoshida, N.; Suzuki, S.; Kameshima, Y.; Nakajima, A. *Surf. Sci.* **2006**, *600*, 2711−2717.
(65) Suzuki, S.; Nakajima, A.; Tanaka, K.; Sakai, M.; Hashimoto, A.; Yoshida, N.; Kameshima, Y.; Okada, K. *Appl. Surf. Sci.* **2008**, *254*, 1797−1805.
(66) Nosonovsky, M.; Bhushan, B. *J. Phys.: Condens. Matter* **2008**, 20.